

Information Restrain in Open Quantum Systems

Chun-Hui Liu^{1,2} and Shu Chen^{1,2,3,*}

¹*Beijing National Laboratory for Condensed Matter Physics,
Institute of Physics, Chinese Academy of Sciences, Beijing 100190, China*

²*School of Physical Sciences, University of Chinese Academy of Sciences, Beijing 100049, China*

³*Yangtze River Delta Physics Research Center, Liyang, Jiangsu 213300, China*

Non-Hermitian skin effect of Liouvillian superoperators in quantum open systems can induce phenomena of non-trivial damping, known as chiral/helical damping. While non-Hermitian skin effect and chiral/helical damping occur only under open boundary condition, we propose an effect called information restrain which does not rely on boundary conditions. We demonstrate that information restrain is stable against disorder and is an intrinsic property of a type of open quantum systems or non-Hermitian system. Then we define the strength of information restrain I_R , which describes the ratio of different decay rates of signal's strengths along opposite propagation directions. Based on information restrain, We can provide a simple and elegant explanation of chiral and helical damping, and get the local maximum of relative particle number for periodical boundary system, consistent with numerical calculations. In terms of information restrain, we also illustrate the existence of correspondence between edge modes and damping modes and deduce that there are many chiral/helical transport properties in this 'information restrain' class.

I. INTRODUCTION

Many open quantum systems can be effectively described by non-Hermitian matrix or Hamiltonian, e.g., the short time evolution of the Lindblad master equation Eq.(1) is governed by non-Hermitian Hamiltonian $H_{NH} = H - i \sum_{\mu} L_{\mu}^{\dagger} L_{\mu}$ before the occurrence of first quantum jump¹⁻⁴. Essentially, the Lindblad master equation can be mapped to a non-Hermitian 'Schrödinger equation' even with quantum jump term after using a basis to represent the density matrix⁵⁻⁹, and the calculating the Lindbladian spectrum of the superoperator can always be viewed as a non-Hermitian eigenvalue problem. Particles with finite lifetime can also be effectively described by non-Hermitian Hamiltonian. Non-Hermitian systems have been unveiled to possess some unique features, such as non-Hermitian skin effect¹⁰⁻²⁴, exceptional points²⁵⁻³¹ and amplified symmetry classes³²⁻³⁷. These unique features produce significant influence on the time evolution of the system and give rise to some peculiar dynamical phenomena, such as chiral/helical damping for non-Hermitian skin effect^{38,39} and amplifying sensors for exceptional points⁴⁰⁻⁴³.

The non-Hermitian skin effect relies on the boundary condition, and no non-Hermitian skin effect can be observed for systems under periodic boundary condition (PBC). Similarly, the phenomena of chiral and helical damping in quantum open systems occurs only under the open boundary condition. An important issue is to extract the intrinsic property for systems exhibiting non-Hermitian skin effect, and get a unique feature which is not sensitive to boundary condition. We expect that this feature can explain chiral/helical damping without resorting to non-Hermitian skin effect.

In this work, we propose an effect called information restrain which is defined by the strength of signal having different decay rate along opposite propagation directions. The ratio of strengths propagating along opposite

directions defines the strength of information restrain I_R . Based on information restrain, we get a simple and elegant explanation of helical and chiral damping, and are able to analytically calculate the local maximum of relative particle number, which is consistent with numerical calculation. The non-Hermitian skin effect also can explain helical and chiral damping, but it needs more complex calculation and only works under open boundary condition (OBC)^{38,39}. Instead, the information restrain exists even under PBC, which does not support the non-Hermitian skin effect. Based on information restrain, we illustrate the existence of correspondence between edge modes and damping modes. An important deduction is that there are many chiral/helical transport properties in this 'information restrain' class (a type of open quantum system), such as chiral/helical thermal transport and chiral/helical electric conductance, which deserve further study.

II. INFORMATION RESTRAIN

To illustrate the concept of information restrain, we study the particle transport in open Su-Schrieffer-Heeger (SSH) chain and demonstrate that the information restrain is an intrinsic property of a type of open quantum systems. Consider the open Markovian quantum systems described by the Lindblad master equation

$$\frac{d\rho}{dt} = \mathcal{L}[\rho] = -i[H, \rho] + \sum_{\mu} (2L_{\mu}\rho L_{\mu}^{\dagger} - \{L_{\mu}^{\dagger}L_{\mu}, \rho\}), \quad (1)$$

where ρ is the density matrix, L_{μ} are Lindblad operators describing quantum jump processes, and H is the Hamiltonian. Particularly, we consider the SSH model with the Hamiltonian in the momentum space given by

$$h(k) = (t_1 + t_2 \cos k)\sigma_x + t_2 \sin k \sigma_y \quad (2)$$

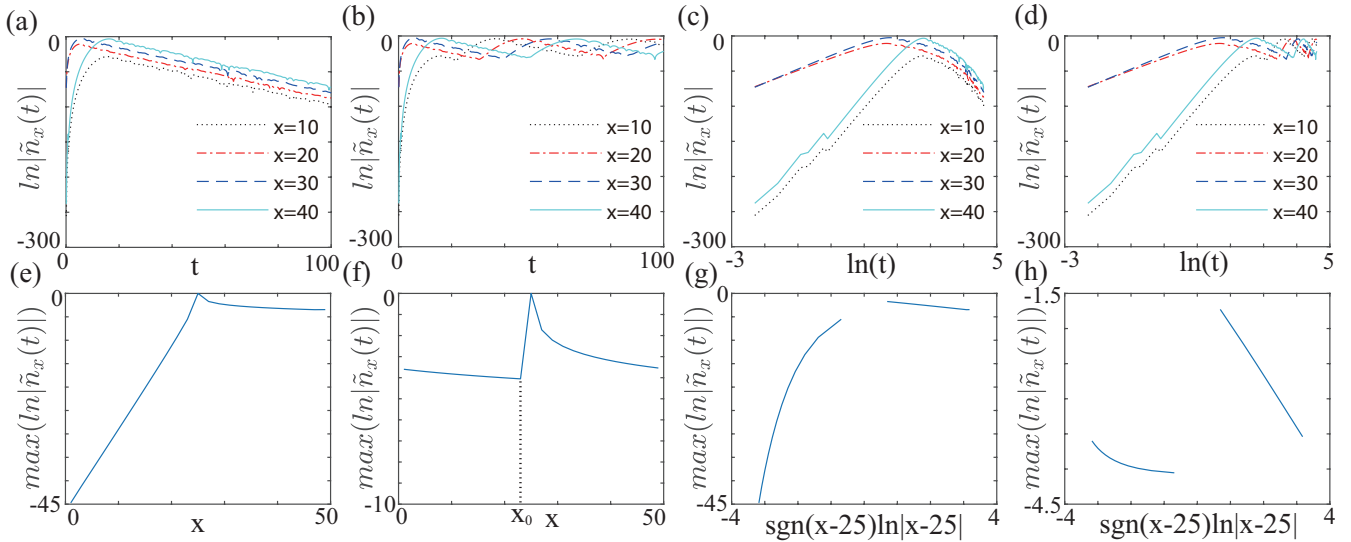


FIG. 1: (a)(c)The evolution of $|\tilde{n}_x(t)|$ at cells $x = 10, 20, 30$ and 40 under OBC. (b)(d) The evolution of $|\tilde{n}_x(t)|$ at cells $x = 10, 20, 30$ and 40 under PBC. $max_x(|\tilde{n}_x(t)|)$ as a function of x under OBC (e)(g) and PBC (f)(h). The parameters are $t_1 = t_2 = 1$ and $\gamma = 0.8$.

where t_1 and t_2 represent the hopping amplitude in and between the unit cells, respectively, and there are two (A and B) sublattices in each cell. The coupling to the environment is described by the Lindblad operators given by

$$L_x^l = \sqrt{\frac{\gamma}{2}}(c_{xA} - ic_{xB}). \quad (3)$$

The dynamics of Green function $\Delta_{ij} = Tr(\rho c_i^\dagger c_j)$ is governed by

$$\tilde{\Delta} = \Delta - \Delta_s = e^{Xt} \tilde{\Delta}(0) e^{X^\dagger t},$$

where Δ_s is the steady value of Δ and X is damping matrix with the matrix in the momentum space given by

$$X(k) = ih(k) + \frac{\gamma}{2}\sigma_y - \frac{\gamma}{2}\sigma_0.$$

The diagonal elements of $\tilde{\Delta}$ give the relative particle number defined by $\tilde{n}_x(t) = \tilde{\Delta}_{xA,xA} + \tilde{\Delta}_{xB,xB}$. Suppose that a particle is initially prepared at the site $25B$ and the system size is 50 , we have $\tilde{\Delta}_{25B,25B}(0) = 1$ and $\tilde{\Delta}_{m,n}(0) = 0$ when m or $n \neq 25B$. It can be recognized as a signal initially input at site $25B$. We numerically calculate the relative particle number $\tilde{n}_x(t)$ versus t in Figs.(1) (a)-(d). Figs.(1a) and (1c) show the evolution of $\tilde{n}_x(t)$ at $x = 10, 20, 30$ and 40 under OBC. For a fixed x , $\tilde{n}_x(t)$ increases in a power law to the maximum value $max(\tilde{n}_x)$ at $t_{max}(x)$, and exponentially decreases after $t_{max}(x)$. The $t_{max}(x)$ can be recognized as the time when the signal reaches x , and $max(\tilde{n}_x)$ is the strength of the signal. As $max(\tilde{n}_x)$ is a single-value function of x , we illustrate it in Figs.1(e) and 1(g). While the signal's

strength decreases exponentially when propagating along $-x$ direction ($x \rightarrow x - 1$), it exhibits a power-law decay along $+x$ direction ($x \rightarrow x + 1$). The signal's strength has different decay rate in opposite direction, and we dub this phenomenon as 'information restrain'. We also numerically calculate the velocity of the signal propagation and get $v = 1$, which equals to the maximum fermi velocity of $X(k)$.

Information restrain does not rely on the boundary condition. Figs.1(b) and 1(d) show the evolution of $\tilde{n}_x(t)$ at $x = 10, 20, 30$ and 40 under PBC, which exhibits the same behavior as under OBC at the early time. We illustrate $max(\tilde{n}_x)$ versus x in Fig.(1f), indicating that the signal's strength decreases exponentially along $-x$ direction ($x \rightarrow x - 1$) and in a power law along $+x$ direction ($x \rightarrow x + 1$). At site $x = x_0$, the propagating signal along the $+x$ direction and $-x$ direction have the same strength. At site $x \in (x_0, 25)$ propagating signal along the $-x$ direction has bigger strength than the propagating signal along the $+x$ direction, and $max(\tilde{n}_x)$ is an exponential function of x . At site $x \in (1, x_0) \cup (25, 50)$, propagating signal along the $+x$ direction has bigger strength than the signal propagating along the $-x$ direction, and $max(\tilde{n}_x)$ is a power-law function of x . It is clear that information restrain also occurs under PBC.

With the increase in time, the evolution of $\tilde{n}_x(t)$ has many local maximums under PBC. For $x = 10$ and 20 , the local maximum is found at $t_{locmax} = 25 - x$ and $x + 25 + 50N$, where N is an integer. For $x = 30$ and 40 , the local maximum is at $t_{locmax} = x - 25 + 50N$. This can be understood in terms of information restrain. If $x \in (1, 25)$, the signal propagates along the $-x$ direction and reaches x at time $t = \frac{25-x+50N}{v}$. Meanwhile, the signal propagates along the $+x$ direction and reaches

x at time $t = \frac{x+25+50N}{v}$. The signal from the $-x$ direction will be covered by the one from $+x$ direction after $t = \frac{x+25-\Delta_x}{v}$ (Δ_x is the effect of signal's width and $\Delta_x \in (0, 4)$), because the strength of signal from the $+x$ direction exhibits a power-law decay and from the $-x$ direction fulfills an exponential decay. Taking account of $v = 1$, we get the local maximum at $t_{locmax} = 25 - x$ and $x + 25 + 50N$ for $x = 10$ and 20 .

If $x \in (25, 50)$, the signal propagates along the $-x$ direction and reaches x at time $t = \frac{75-x+50N}{v}$. The signal propagates along $+x$ direction and reaches x at time $t = \frac{x-25+50N}{v}$. The signal from the $-x$ direction will be covered by the signal from the $+x$ direction after $t = \frac{x-25-\Delta_x}{v}$. Due to $v = 1$, we get the local maximum at $t_{locmax} = x - 25 + 50N$.

In Ref.^{38,39}, the chiral/helical damping was unveiled to occur in the quantum open systems when the damping matrix exhibits non-Hermitian skin effect. Both chiral/helical damping and non-Hermitian skin effect rely on the open boundary condition and thus are not intrinsic properties of the system. Instead, information restrain can provide a simple and elegant way to understand the chiral and helical damping, as the information restrain does not rely on boundary condition and thus is an intrinsic property of the system. For the chiral damping case, supposing that the system is fully filled at the initial time and $v = 1$, the particle propagating along the $-x$ direction decays exponentially and the one along the $+x$ direction decays in power law. Particle propagating along the $+x$ direction will arrive in the site x at time $t \in (0, x)$, and \tilde{n}_x decays in a power law for $t \in (0, x)$. After $t = x$, no information from the particle propagating from the $+x$ direction will be received, and then \tilde{n}_x exponentially decays for $t \in (x, \infty)$. In the helical damping case, there are two channels labeled as α and β . In the α channel, particle propagating along the $-x$ direction is exponentially decaying, and particle propagating along $+x$ direction exhibits a power-law decay behavior. On the other hand, β channel's decay behavior is opposite to that of α channel since it fulfills time reverse symmetry. Then \tilde{n}_x has a sharp decrease at time $t = x$ and $L - x$. For open systems with their damping matrix having skin effect, the information restrain can be always observed independent of the boundary condition.

The information restrain also exists in the spin chain. Consider the Lindblad master equation with the Hamiltonian described by

$$h = \sum_{j=1}^N J_1(\sigma_{2j-1}^x \sigma_{2j}^x + \sigma_{2j-1}^y \sigma_{2j}^y) + \sum_{j=1}^{N-1} J_2(\sigma_{2j}^x \sigma_{2j+1}^x + \sigma_{2j}^y \sigma_{2j+1}^y) \quad (4)$$

and the Lindblad operators given by

$$L_j = \sqrt{g}(\sigma_{2j}^- + i\sigma_{2j+1}^-). \quad (5)$$

If we omit the quantum jump term in the master equation, the evolution of density matrix is governed by

$\rho(t) = e^{-iH_{NH}t}\rho(0)e^{iH_{NH}^\dagger t}$ with $H_{NH} = h - i\sum_j L_j^\dagger L_j$. After the Jordan-Wigner transformation,

$$H_{NH} = \sum_{j=1}^{2N} -iga_j^\dagger a_j + \sum_{j=1}^N [(2J_1 - g)a_{2j-1}^\dagger a_{2j} + (2J_1 + g)a_{2j}^\dagger a_{2j-1}] + \sum_{j=1}^{N-1} [2J_2 a_{2j}^\dagger a_{2j+1} + h.c.] \quad (6)$$

Particle number is conserved under the evolution of H_{NH} . If particle number is 1 at the initial time, we just need to consider single particle Fock space with basis $|1\rangle, |2\rangle, \dots, |2N\rangle$. Since H_{NH} plays a similar role as the damping matrix X under this basis, we can get that information restrain exists in this case by similar calculation and discussion.

III. EFFECT OF DISORDER

Now we study the effect of disorder and illustrate that the information restrain is stable against disorder. We first consider the disorder introduced in the hopping amplitude with the Hamiltonian in the Lindblad equation described by

$$H = \sum_i [t_1 c_{i,A}^\dagger c_{i,B} + (t_2 + Wr_i) c_{i,B}^\dagger c_{i+1,A} + h.c.], \quad (7)$$

where $r_i \in (0, 1)$ is a random variable and W is the strength of disorder. The Lindblad operator is given by Eq.(3) with the initial state the same as the case in the absence of disorder. We numerically calculate $max(\tilde{n}_x)$ under the OBC, which is illustrated in Fig(2a) and (2b). It is shown that the information restrain exists for both $W = 1$ and $W = 10$. Then we consider random disorder in chemical potential with the Hamiltonian described by

$$H = \sum_i [t_1 c_{i,A}^\dagger c_{i,B} + t_2 c_{i,B}^\dagger c_{i+1,A} + h.c. + Wr_i c_{i,A}^\dagger c_{i,A}] \quad (8)$$

and Lindblad operator is the same as Eq.(3). Similarly, we numerically illustrate $max(\tilde{n}_x)$ under OBC in Fig(2c) and (2d). The information restrain exists for $W = 1$. With the increase of W , the information restrain is suppressed, but there still exists signature of different decaying rate in different propagating direction even for $W = 100$. Our results indicate that the information restrain is robust against the disorder.

IV. STRENGTH OF INFORMATION RESTRAIN

In order to describe information restrain quantitatively, next we define the strength of information restrain

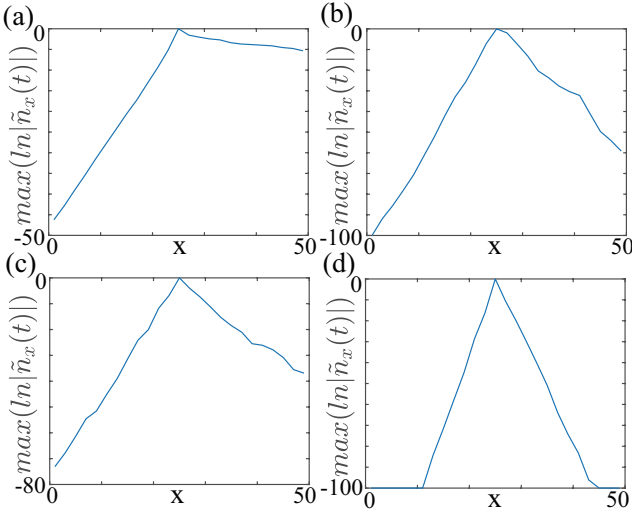


FIG. 2: $\max(|\tilde{n}_x|)$ as a function of x under OBC. (a) and (b) correspond to the model of Eq.(7) with disorder strength $W = 1$ and $W = 10$, respectively. (c) and (d) correspond to the model of Eq.(8) with disorder strength $W = 10$ and $W = 100$, respectively. The other parameters are $t_1 = t_2 = 1$ and $\gamma = 0.8$.

as

$$I_R(j_1, j_2, t) = \frac{I_+}{I_-}, \quad (9)$$

where I_+ (I_-) represents the strength of information propagating along the $+$ ($-$) direction. In our previous discussion, it represents charge transport and is defined as

$$\begin{aligned} I_+ &= \text{Tr} [e^{\mathcal{L}t} [|j_1\rangle\langle j_1|] |j_2\rangle\langle j_2|], \\ I_- &= \text{Tr} [e^{\mathcal{L}t} [|j_2\rangle\langle j_2|] |j_1\rangle\langle j_1|]. \end{aligned} \quad (10)$$

To calculate I_R , we have

$$\begin{aligned} I_+ &= \langle\langle j_2 | e^{Xt} | j_1 \rangle\rangle \langle\langle j_1 | e^{X^\dagger t} | j_2 \rangle\rangle, \\ I_- &= \langle\langle j_1 | e^{Xt} | j_2 \rangle\rangle \langle\langle j_2 | e^{X^\dagger t} | j_1 \rangle\rangle. \end{aligned} \quad (11)$$

where $j_1, j_2 = 1A, 1B, \dots, 50B$ are lattice site indexes, $|j_1\rangle\rangle$ and $|j_2\rangle\rangle$ are matrix representations of $|j_1\rangle$ and $|j_2\rangle$ in the single particle basis $[|1A\rangle, |1B\rangle, \dots, |50B\rangle]$, and $\langle\langle j_1|$ and $\langle\langle j_2|$ are Hermitian conjugations of $|j_1\rangle\rangle$ and $|j_2\rangle\rangle$. Taking $j_1 = 25B$, $j_2 = 25 + mB$ ($m > 0$) and $X = S(-\frac{\gamma}{2}\mathbb{I} + iH_{SSH})S^{-1}$ in the above expressions, where H_{SSH} is the matrix representation of the SSH Hamiltonian in the single particle basis with two hopping parameters $\tilde{t}_1 = \sqrt{(t_1 - \frac{\gamma}{2})(t_1 + \frac{\gamma}{2})}$ and $\tilde{t}_2 = t_2$, $S = \text{diag}[1, \beta, \beta, \dots, \beta^{L-1}, \beta^L]$ and $\beta = \sqrt{\frac{t_1 + \gamma/2}{t_1 - \gamma/2}}$, we get that $I_+ = e^{2\ln(\beta)m - \gamma t \mathbb{I}} |\langle\langle 25 + mB | e^{iH_{SSH}t} | 25B \rangle\rangle|^2$, $I_- = e^{-2\ln(\beta)m - \gamma t \mathbb{I}} |\langle\langle 25B | e^{iH_{SSH}t} | 25 + mB \rangle\rangle|^2$ and $I_R \approx \beta^{4m} \approx e^{1.69m}$. From Fig.(1f), we numerically calculate $\max(\tilde{n}_{25+m})/\max(\tilde{n}_{25-m}) = e^{1.72m}$, and it is approximately equal to I_R . It illustrates that I_R can describe

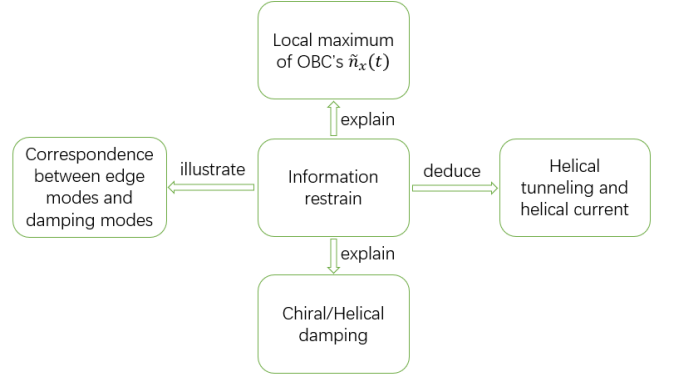


FIG. 3: Schematic diagram of main conclusions.

the different decay rate of signal's strength propagating along opposite direction. In fact, the signal's strength can be represented by $I_{\pm}(j_2 - j_1 = vt)$ with $v = 1$ being the Fermi velocity, because the signal propagates from j_1 to $j_1 + vt$ after the time of t . In the appendix A, we illustrate that it is equivalent to defining I_{\pm} as

$$\begin{aligned} I_+ &= \left| \text{Tr} \left[\left\{ c_{j_2}(t), c_{j_1}^\dagger(0) \right\} \rho_{NESS} \right] \right|^2, \\ I_- &= \left| \text{Tr} \left[\left\{ c_{j_1}(t), c_{j_2}^\dagger(0) \right\} \rho_{NESS} \right] \right|^2, \end{aligned} \quad (12)$$

where ρ_{NESS} is the non-equilibrium steady density matrix, $c_{j_1}^\dagger(0)$ and $c_{j_2}(t)$ are creation and annihilation operators which satisfy the following equation:

$$\frac{dO}{dt} = \mathcal{L}^\dagger[\rho] = i[H, O] + \sum_{\mu} (2L_{\mu}^\dagger O L_{\mu} - \{L_{\mu}^\dagger L_{\mu}, O\}). \quad (13)$$

I_{\pm} represent the square of the absolute value of Green's function. The definition given by Eq.(12) can be applied to calculate the interacting system and thus their ratio I_R can be used to characterize the information restrain in many-body systems. Similarly, we can define I_{\pm} by spin transport for the spin model.

We can define a local quantity $r(j) = \ln(I_R(j, j + m, t))/m$, where $m = 1$ for lattice models and $m \rightarrow 0$ for continuous models. The $r(j)$ is not sensitive to the boundary condition, and the physical origin of this property is that the master equation is a local master equation which does not include long-range terms. As long as there is a ρ_{NESS} , $r(j)$ is well defined, and thus is universal.

V. SUMMARY AND DISCUSSION

In summary, we proposed an effect coined information restrain which is an intrinsic property of a type of open quantum systems independent of the boundary condition. We define the strength of information restrain I_R and illustrate that it can effectively describe the different decay rate of signal's strength propagating along opposite direction. Our calculation demonstrates that the

information restrain is stable against disorder. Based on information restrain, we can get a simple and elegant explanation for the chiral and helical damping, and also get the local maximum \tilde{n}_x of the periodic system, which is consistent with the numerical calculation.

Based on information restrain, many physical phenomena can be predicted and understood in a unified way. Due to the information is carried by particles, if one of channels has information restrain, all transport property will have a restrain direction in this channel. Hence chiral/helical thermal transport and chiral/helical electric conductance are expected to exist widely in open quantum systems. Particularly, we can demonstrate the correspondence between edge modes and damping modes based on information restrain. An example is the correspondence between the existence of chiral/helical edge modes in topological insulator⁴⁴⁻⁴⁷ and chiral/helical damping in quantum open systems^{38,39} (see Appendix B for details). In general, if there are η type (η can be chiral/helical or others) edge modes, then the information restrain belongs to the η type for these edge modes. Correspondingly, there are η type damping modes accord-

ing to our information restrain explanation of damping modes. An important deduction is that many chiral and helical transport properties can be explained in a unified way in terms of information restrain as displayed in Fig(3), which schematically summarize our main conclusions. One of the helical transport properties is helical tunneling effect, which describes the phenomenon that particles with opposite spins belonging to different channels have opposite restrain direction (see Appendix C for details).

Acknowledgments

C.-H. Liu would thank K. Zhang, Z. Yang and Z. Wang for very helpful discussions. The work is supported by the National Key Research and Development Program of China (2016YFA0300600 and 2016YFA0302104), NSFC under Grants No.11974413 and the Strategic Priority Research Program of Chinese Academy of Sciences under Grant No. XDB33000000.

Appendix A: Prove the equivalence of Eq.[10] and Eq.[12]

In Schrödinger picture, the operators do not evolve with time and the density matrix satisfies Eq.(1). The solution of Lindblad equation can be formally represented as $\rho(t) = e^{\mathcal{L}t}[\rho]$, where $e^{\mathcal{L}t} = \sum_{n=0}^{\infty} \frac{(\mathcal{L}t)^n}{n!}$. In Heisenberg picture, the density matrix does not evolve with time and the operators satisfy Eq.(13). It follows $O(t) = e^{\mathcal{L}^\dagger t}[O]$, where $e^{\mathcal{L}^\dagger t} = \sum_{n=0}^{\infty} \frac{(\mathcal{L}^\dagger t)^n}{n!}$. In the main text, $\rho_{NESS} = |NESS\rangle\langle NESS| = |0\rangle\langle 0|$ is the density matrix without any particles. By setting $j_1 = 25B$, $j_2 = 25 + mB$ in Eq.(12), we have

$$\begin{aligned}
I_+ &= |\langle 0|(c_{25+mB}(t)c_{25B}^\dagger(0) + c_{25B}^\dagger(0)c_{25+mB}(t))|0\rangle|^2 \\
&= |\langle 0|c_{25+mB}(t)c_{25B}^\dagger(0)|0\rangle|^2 \\
&= |\langle 0|e^{\mathcal{L}^\dagger t}[c_{25+mB}(0)]|25B\rangle|^2 \\
&= |Tr \left\{ |25B\rangle\langle 0|e^{\mathcal{L}^\dagger t}[c_{25+mB}(0)] \right\}|^2 \\
&= |Tr \left\{ e^{\mathcal{L}t}[|25B\rangle\langle 0|]c_{25+mB}(0) \right\}|^2 \\
&= |Tr \left\{ e^{-iH_{eff}t}|25B\rangle\langle 0|c_{25+mB}(0) \right\}|^2 \\
&= |Tr \left\{ e^{-iH_{eff}t}|25B\rangle\langle 25 + mB| \right\}|^2 \\
&= |\langle 25 + mB|e^{-iH_{eff}t}|25B\rangle|^2,
\end{aligned} \tag{A1}$$

Similarly,

$$I_- = |\langle 25B|e^{-iH_{eff}t}|25 + mB\rangle|^2,$$

where $H_{eff} = H - i \sum_{x=1}^{50} L_x^\dagger L_x$. In the single particle basis $|1A\rangle, |1B\rangle, \dots, |50B\rangle$, Eq.(A1) is equivalent to Eq.(10). In the derivation of Eq.(A1), we use two relations:

$$Tr[Pe^{\mathcal{L}^\dagger t}[Q]] = Tr[e^{\mathcal{L}t}[P]Q], \tag{A2}$$

and

$$e^{\mathcal{L}t}[|25B\rangle\langle 0|] = e^{-iH_{eff}t}|25B\rangle\langle 0|. \tag{A3}$$

Proof of Eq.(A2): It is easy to verify that $Tr[P\mathcal{L}^\dagger[Q]] = Tr[\mathcal{L}[P]Q]$, then we have $Tr[P\mathcal{L}^{\dagger n}[Q]] = Tr[\mathcal{L}^n[P]Q]$.

$$\begin{aligned} Tr[Pe^{\mathcal{L}^\dagger t}[Q]] &= \sum_{n=0}^{\infty} \frac{t^n}{n!} Tr[P\mathcal{L}^{\dagger n}[Q]] \\ &= \sum_{n=0}^{\infty} \frac{t^n}{n!} Tr[\mathcal{L}^n[P]Q] \\ &= Tr[e^{\mathcal{L}t}[P]Q] \end{aligned} \quad (\text{A4})$$

Proof of Eq.(A3): We begin with

$$\begin{aligned} \mathcal{L}[|25B\rangle\langle 0|] &= -i[H, |25B\rangle\langle 0|] + \sum_x (2L_x^l |25B\rangle\langle 0| L_x^{l\dagger} - \{L_x^{l\dagger} L_x^l, |25B\rangle\langle 0|\}) \\ &= (-iH - \sum_x L_x^{l\dagger} L_x^l) |25B\rangle\langle 0|. \end{aligned} \quad (\text{A5})$$

Here we use $\langle 0|H = 0$ and $\langle 0|L_x^{l\dagger} = 0$. Assume that

$$\mathcal{L}^n[|25B\rangle\langle 0|] = (-iH - \sum_x L_x^{l\dagger} L_x^l)^n |25B\rangle\langle 0|, \quad (\text{A6})$$

then we get

$$\begin{aligned} \mathcal{L}^{n+1}[|25B\rangle\langle 0|] &= \mathcal{L}[(-iH - \sum_x L_x^{l\dagger} L_x^l)^n |25B\rangle\langle 0|] \\ &= -i[H, (-iH - \sum_x L_x^{l\dagger} L_x^l)^n |25B\rangle\langle 0|] + \sum_x (2L_x^l (-iH - \sum_x L_x^{l\dagger} L_x^l)^n |25B\rangle\langle 0| L_x^{l\dagger} \\ &\quad - \left\{ L_x^{l\dagger} L_x^l, (-iH - \sum_x L_x^{l\dagger} L_x^l)^n |25B\rangle\langle 0| \right\}) \\ &= (-iH - \sum_x L_x^{l\dagger} L_x^l)^{n+1} |25B\rangle\langle 0|. \end{aligned} \quad (\text{A7})$$

Combining Eq.(A5), (A6) and (A7), we conclude that Eq.(A6) holds true for any n . Finally we get

$$\begin{aligned} e^{\mathcal{L}t}[|25B\rangle\langle 0|] &= \sum_{n=0}^{\infty} \frac{t^n}{n!} \mathcal{L}^n[|25B\rangle\langle 0|] \\ &= \sum_{n=0}^{\infty} \frac{t^n}{n!} (-iH - \sum_x L_x^{l\dagger} L_x^l)^n |25B\rangle\langle 0| \\ &= e^{-iH_{eff}t} |25B\rangle\langle 0|. \end{aligned} \quad (\text{A8})$$

Appendix B: Correspondence between damping modes and edge modes

We first discuss the analogy of edge modes to damping modes. Consider the edge state of a quantum anomalous Hall system (For example, Haldane model), which is described by effective Hamiltonian:

$$H_{e1} = \alpha \hat{k} \quad (\text{B1})$$

The site x is fully occupied for $0 < x < L$ and empty for $x < 0$ and $x > L$ at the initial time, as illustrated in Fig.(4a). We take $0 < x < L$ as the system, and $x < 0$ and $x > L$ as the bath. Because $e^{-iH_{e1}}|x\rangle = |x + \alpha t\rangle$, the particle number of system $n_x(t)$ satisfies that:

$$n_x(t) = \begin{cases} 2, & x > \alpha t, \\ 0, & x < \alpha t. \end{cases} \quad (\text{B2})$$

The unidirectional distribution of particle number exhibits similar behavior of chiral damping.

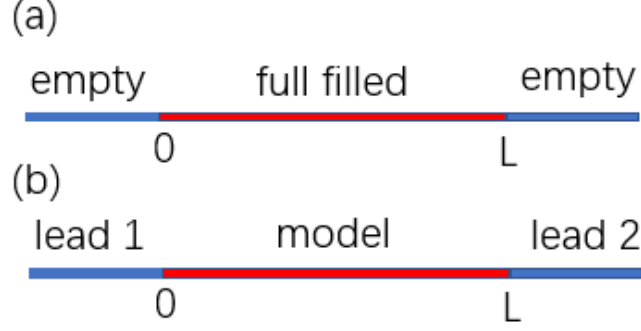


FIG. 4: (a) Schematic diagram of edge modes. (b) Schematic diagram of chiral current.

Next we discuss the analogy of damping modes to edge modes. Consider the model described by Eqs.(2)and (3)and a setup illustrated in Fig.(4b) with the system region of $0 < x < L$ and the lead region of $x < 0$ and $x > L$. If we omit the contact resistance and lead resistance. Because of Eqs.(9),(10) and $I_R \approx \beta^{4L}$ (for $j_2 - j_1 = vt = L$), we have $T_{12} \approx \beta^{4L} T_{21}$. Substitute it into Landauer-Buttiker formalism,

$$I_i = \frac{e^2}{h} \sum_{i \neq j} [T_{ji} V_i - T_{ij} V_j], \quad (\text{B3})$$

where i, j is the lead index. For $V_1 = V_2 = V$, we get that $I_1 \approx -\frac{e^2}{h} (\beta^{4L} - 1) T_{21} V \approx -\frac{e^2}{h} \beta^{4L} T_{21} V \neq 0$. The chiral current exhibits similar behavior to the edge of two-dimensional quantum anomalous hall effect. However, it is induced by the non-unitarity of the scattering matrix. We can estimate the value of T_{21} .

$$\begin{aligned} T_{21} &\propto \langle \langle 1A | e^{Xt} | LB \rangle \rangle \langle \langle LB | e^{X^\dagger t} | 1A \rangle \rangle \\ &= \langle \langle 1A | e^{S(iH_{SSH} - \frac{\gamma}{2}\mathbb{I})S^{-1}\frac{L}{v}} | LB \rangle \rangle \langle \langle LB | e^{S^{-1}(-iH_{SSH} - \frac{\gamma}{2}\mathbb{I})S\frac{L}{v}} | 1A \rangle \rangle \\ &= \langle \langle 1A | S e^{(iH_{SSH} - \frac{\gamma}{2}\mathbb{I})L} S^{-1} | LB \rangle \rangle \langle \langle LB | S^{-1} e^{(-iH_{SSH} - \frac{\gamma}{2}\mathbb{I})L} S | 1A \rangle \rangle \\ &= \beta^{-2L} e^{-\gamma L} \langle \langle 1A | e^{iH_{SSH}L} | LB \rangle \rangle \langle \langle LB | e^{-iH_{SSH}L} | 1A \rangle \rangle \\ &\approx \beta^{-4L} \langle \langle 1A | e^{iH_{SSH}L} | LB \rangle \rangle \langle \langle LB | e^{-iH_{SSH}L} | 1A \rangle \rangle. \end{aligned} \quad (\text{B4})$$

Here we use $t = \frac{L}{v}$, $v = 1$, $X = S(-\frac{\gamma}{2}\mathbb{I} + iH_{SSH})S^{-1}$, $S = \text{diag}[1, \beta, \beta, \dots, \beta^{L-1}, \beta^L]$ and $\beta = \sqrt{\frac{t_1 + \gamma/2}{t_1 - \gamma/2}}$. H_{SSH} is the matrix representation of the SSH Hamiltonian in the single particle basis with two hopping parameters $\tilde{t}_1 = \sqrt{(t_1 - \frac{\gamma}{2})(t_1 + \frac{\gamma}{2})}$ and $\tilde{t}_2 = t_2$.

Appendix C: Helical current and helical tunneling effect

Consider the model discussed in Ref.³⁹. For convenience, here we write this model explicitly with the Hamiltonian described by

$$h(k) = t_1 \sigma_x + (t_2 \sigma_y + \delta_1 \tau_x) \sin k + t_2 \sigma_x \cos k + \delta_2 \sigma_z \tau_x, \quad (\text{C1})$$

and the Lindblad operators

$$\begin{aligned} L_{x\uparrow}^l &= \sqrt{\frac{\gamma l}{2}} (c_{xA\uparrow} - i c_{xB\uparrow}), & L_{x\uparrow}^g &= \sqrt{\frac{\gamma g}{2}} (c_{xA\uparrow}^\dagger + i c_{xB\uparrow}^\dagger), \\ L_{x\downarrow}^l &= \sqrt{\frac{\gamma l}{2}} (c_{xA\downarrow} + i c_{xB\downarrow}), & L_{x\downarrow}^g &= \sqrt{\frac{\gamma g}{2}} (c_{xA\downarrow}^\dagger - i c_{xB\downarrow}^\dagger). \end{aligned} \quad (\text{C2})$$

The damping matrix is

$$\begin{aligned}
X &= i \begin{bmatrix} H_{nSSH}(k) + \frac{i\gamma}{2} & \delta_1 \sin k \\ \delta_1 \sin k & H_{nSSH}^T(-k) + \frac{i\gamma}{2} \end{bmatrix} \\
&= \left(-\frac{\gamma}{2} + it_1\sigma_x + \frac{\gamma}{2}\sigma_y\tau_z\right) + i(t_2\sigma_y + \delta_1\tau_x) \sin k \\
&\quad + it_2\sigma_x \cos k + i\delta_2\sigma_z\tau_x.
\end{aligned} \tag{C3}$$

which fulfills

$$CX(-k)^T = X(k)C \tag{C4}$$

with $C = i\tau_y$. First, we consider the case $\delta_1 = 0$. Consider the similar problem in the last section as illustrated in Fig.(4b) and $V_1 = V_2 = V$, the spin up fermion forms a current $I_\uparrow = -\frac{e^2}{h}\beta^{4L}T_{21}V$ and the spin down fermion forms a current $I_\downarrow = \frac{e^2}{h}\beta^{4L}T_{21}V$. The total spin current is not zero and equal to $I^s = \frac{\hbar/2}{e}(I_\uparrow - I_\downarrow) = -\frac{e}{4\pi}\beta^{4L}T_{21}V$. Then, we consider the case $\delta_1 \neq 0$. We add some perturbations and the GBZ equation does not change, then the GBZ is a continuous function of the perturbations. The eigenvalues and eigenstates of X are continuous functions of the GBZ, it is also continues function of this perturbation (which is discussed in ref^[39], we follow the explanation here). Then the helical current is stable against this perturbation.

Given that $\tilde{n}_{(x_1, s_1, o_1) \rightarrow (x, s, o)}$ and $\tilde{n}_{(x_1, s_1, o_1) \rightarrow (x, s, o), k+i\kappa}$ are defined as

$$\tilde{n}_{(x_1, s_1, o_1) \rightarrow (x, s, o)} = \langle\langle (x, s, o) | e^{Xt} | (x_1, s_1, o_1) \rangle\rangle \langle\langle (x_1, s_1, o_1) | e^{X^\dagger t} | (x, s, o) \rangle\rangle \tag{C5}$$

and

$$\tilde{n}_{(x_1, s_1, o_1) \rightarrow (x, s, o), k+i\kappa} = \langle\langle (x, s, o) | e^{X(k+i\kappa)t} | (x_1, s_1, o_1) \rangle\rangle \langle\langle (x_1, s_1, o_1) | e^{X^\dagger(k+i\kappa)t} | (x, s, o) \rangle\rangle, \tag{C6}$$

we can get $\tilde{n}_{(x_1, s_1, o_1) \rightarrow (x, s, o), k+i\kappa}$ using similar method in the appendix of ref^[39]:

$$\begin{aligned}
\tilde{n}_{(x_1, s_1, o_1) \rightarrow (x, s, o), k+i\kappa} &= \langle\langle (x, s, o) | e^{X(k+i\kappa)t} | (x_1, s_1, o_1) \rangle\rangle \langle\langle (x_1, s_1, o_1) | e^{X^\dagger(k+i\kappa)t} | (x, s, o) \rangle\rangle \\
&= \langle\langle (x, s, o) | e^{X(k+i\kappa)t} | (x_1, s_1, o_1) \rangle\rangle \langle\langle (x_1, s_1, o_1) | e^{X^\dagger(k+i\kappa)t} | (x, s, o) \rangle\rangle \\
&= |\langle\langle (x, s, o) | e^{X(k+i\kappa)t} | (x_1, s_1, o_1) \rangle\rangle|^2 \\
&= \sum_{\alpha} |\langle\langle (x, s, o) | e^{X(k+i\kappa)t} | k+i\kappa, \alpha \rangle\rangle_{RL} \langle\langle k+i\kappa, \alpha | (x_1, s_1, o_1) \rangle\rangle|^2 \\
&= \sum_{\alpha} |\langle\langle (s, o) | \alpha \rangle\rangle_{RL} \langle\langle \alpha | (s_1, o_1) \rangle\rangle e^{i(k+i\kappa)(x-x_1) + \lambda_{k+i\kappa, \alpha} t}|^2 \\
&\propto \sum_{\alpha} |\langle\langle (s, o) | \alpha \rangle\rangle_{RL} \langle\langle \alpha | (s_1, o_1) \rangle\rangle e^{-\kappa(x-x_1) - \frac{\gamma}{2}t}|^2
\end{aligned} \tag{C7}$$

Here we use $|(x, s, o)\rangle\rangle$ and $|(x_1, s_1, o_1)\rangle\rangle$ to denote matrix representation of $|x, s, o\rangle$ and $|x_1, s_1, o_1\rangle$ in the single particle basis $[(1, \uparrow, A), (1, \uparrow, B), \dots, (L, \downarrow, B)]$, α is the band index (corresponding to spin and orbit degree of freedom), $|k+i\kappa, \alpha\rangle\rangle_R = |k+i\kappa\rangle\rangle_R \otimes |\alpha\rangle\rangle_R$ is the eigenstates of $X(k+i\kappa)$. The GBZ components of $\tilde{n}_{(x_1, s_1, o_1) \rightarrow (x, s, o)}$ are $\tilde{n}_{(x_1, s_1, o_1) \rightarrow (x, s, o), k+i\kappa}$ and $\tilde{n}_{(x_1, s_1, o_1) \rightarrow (x, s, o)} = \sum_k \tilde{n}_{(x_1, s_1, o_1) \rightarrow (x, s, o), k+i\kappa}$. Then $\tilde{n}_{(x_1, s_1, o_1) \rightarrow (x, s, o)}$ is dominated by two components:

$$\begin{aligned}
\tilde{n}_{(x_1, s_1, o_1) \rightarrow (x, s, o)} &\propto |\langle\langle (s, o) | \alpha_{max} \rangle\rangle_{RL} \langle\langle \alpha_{max} | (s_1, o_1) \rangle\rangle e^{\kappa_{max}(x_1-x) - \frac{\gamma}{2}t}|^2 \\
&\quad + |\langle\langle (s, o) | \alpha_{min} \rangle\rangle_{RL} \langle\langle \alpha_{min} | (s_1, o_1) \rangle\rangle e^{\kappa_{min}(x_1-x) - \frac{\gamma}{2}t}|^2.
\end{aligned} \tag{C8}$$

Because of the time-reversal symmetry, the spin-orbit components α_{max} and α_{min} have opposite spins and correspondingly $\kappa_{max} = -\kappa_{min} = \kappa_0 > 0$.

If the initial state is $|(x_1, \alpha_{max})\rangle\rangle_R$ and $\tilde{\Delta}(0) = |(x_1, \alpha_{max})\rangle\rangle_{RR} \langle\langle (x_1, \alpha_{max})|$. We can get the tunneling amplitude from $|(x_1, \alpha_{max})\rangle\rangle_R$ to $|(x, \alpha_{max})\rangle\rangle_R$:

$$\begin{aligned}
T_{(x_1, \alpha_{max}) \rightarrow (x, \alpha_{max})} &= Tr [e^{\mathcal{L}t} [| (x_1, \alpha_{max}) \rangle\rangle_{RR} \langle\langle (x_1, \alpha_{max}) | | (x, \alpha_{max}) \rangle\rangle_{RR} \langle\langle (x, \alpha_{max}) |] \\
&= \tilde{n}_{(x_1, \alpha_{max}) \rightarrow (x, \alpha_{max})} \propto e^{2\kappa_0(x_1-x) - \gamma t}
\end{aligned} \tag{C9}$$

If the initial state is at $|(x_1, \alpha_{min})\rangle_R$ and $\tilde{\Delta}(0) = |(x_1, \alpha_{min})\rangle_{RR}\langle(x_1, \alpha_{min})|$, we can get the tunneling amplitude from $|(x_1, \alpha_{min})\rangle_R$ to $|(x, \alpha_{min})\rangle_R$:

$$\begin{aligned} T_{(x_1, \alpha_{min}) \rightarrow (x, \alpha_{min})} &= Tr [e^{\mathcal{L}t} |(x_1, \alpha_{min})\rangle_{RR}\langle(x_1, \alpha_{min})| |(x, \alpha_{min})\rangle_{RR}\langle(x, \alpha_{min})|] \\ &= \tilde{n}_{(x_1, \alpha_{min}) \rightarrow (x, \alpha_{min})} \propto e^{-2\kappa_0(x_1-x) - \gamma t}. \end{aligned} \quad (C10)$$

It means that the restrain direction of α_{min} corresponding to $\kappa_{min} < 0$ is along the $-x$ direction and the restrain direction of α_{max} corresponding to $\kappa_{max} > 0$ is along the $+x$ direction. The restrain direction is defined by signal's strength which has a larger decay rate when propagating along this direction. Because the time-reversal symmetry flips the spin, k and κ at the same time, particles with opposite spins belong to different channels which have opposite restrain directions.

-
- * Electronic address: schen@iphy.ac.cn
- ¹ G. Lindblad, On the generators of quantum dynamical semigroups, *Commun. Math. Phys.* **48**, 119 (1976).
 - ² J. Dalibard, Y. Castin, and K. Molmer, Wave-Function Approach to Dissipative Processes in Quantum Optics, *Phys. Rev. Lett.* **68**, 580 (1992).
 - ³ H.J. Carmichael, Quantum Trajectory Theory for Cascaded Open Systems, *Phys. Rev. Lett.* **70**, 2273 (1993).
 - ⁴ A.J. Daley, Quantum trajectories and open many-body quantum systems, *Adv. Phys.* **63**, 77 (2014).
 - ⁵ S. Diehl, A. Micheli, A. Kantian, B. Kraus, H. P. Buchler, and P. Zoller, Quantum states and phases in driven open quantum systems with cold atoms, *Nat. Phys.* **4**, 878 (2008).
 - ⁶ T. Prosen, Third quantization: a general method to solve master equations for quadratic open Fermi systems, *New J. Phys.* **10**, 043026 (2008).
 - ⁷ T. Prosen, Spectral theorem for the Lindblad equation for quadratic open fermionic systems, *J. Stat. Mech.* (2010) P07020.
 - ⁸ T. Prosen, and E. Ilievski, Nonequilibrium phase transition in a periodically driven xy spin chain, *Phys. Rev. Lett.* **107**, 060403 (2011).
 - ⁹ S. Lieu, M. McGinley, and N. R. Cooper, Tenfold Way for Quadratic Lindbladians, *Phys. Rev. Lett.* **124**, 040401 (2020).
 - ¹⁰ T. E. Lee, Anomalous edge state in a non-hermitian lattice, *Phys. Rev. Lett.* **116**, 133903 (2016).
 - ¹¹ Y. Xiong, Why does bulk boundary correspondence fail in some non-Hermitian topological models, *J. Phys. Commun.* **2**, 035043 (2018).
 - ¹² S. Yao and Z. Wang, Edge States and Topological Invariants of Non-Hermitian Systems, *Phys. Rev. Lett.* **121**, 086803 (2018).
 - ¹³ F. K. Kunst, E. Edvardsson, J. C. Budich, and E. J. Bergholtz, Biorthogonal bulk-boundary correspondence in non-Hermitian systems, *Phys. Rev. Lett.* **121**, 026808 (2018).
 - ¹⁴ S. Yao, F. Song, and Z. Wang, Non-Hermitian Chern Bands, *Phys. Rev. Lett.* **121**, 136802(2018).
 - ¹⁵ C. H. Lee and R. Thomale, Anatomy of skin modes and topology in non-hermitian systems, *Phys. Rev. B* **99**, 201103 (2019).
 - ¹⁶ H. Jiang, L. J. Lang, C. Yang., S. L. Zhu, and S. Chen, Interplay of non-hermitian skin effects and anderson localization in nonreciprocal quasiperiodic lattices, *Phys. Rev. B* **100**, 054301 (2019).
 - ¹⁷ K. Yokomizo and S. Murakami, Non-Bloch Band Theory of Non-Hermitian Systems, *Phys. Rev. Lett.* **123**, 066404 (2019).
 - ¹⁸ K. Zhang, Z. Yang, and C. Fang, Correspondence between winding numbers and skin modes in non-hermitian systems, *Phys. Rev. Lett.* **125**, 126402 (2020).
 - ¹⁹ N. Okuma, K. Kawabata, K. Shiozaki, and M. Sato, Topological Origin of Non-Hermitian Skin Effects, *Phys. Rev. Lett.* **124**, 086801 (2020).
 - ²⁰ D. S. Borgnia, A. J. Kruchkov, R.-J. Slager, Non-Hermitian Boundary Modes, *Phys. Rev. Lett.* **124**, 056802 (2020).
 - ²¹ Z. Yang, K. Zhang, C. Fang, and J. P. Hu, Auxiliary generalized Brillouin zone method in non-Hermitian band theory, *Phys. Rev. Lett.* **125**, 226402 (2020).
 - ²² Y. Yi and Z. Yang, Non-Hermitian skin modes induced by on-site dissipations and chiral tunneling effect, *Phys. Rev. Lett.* **125**, 186802 (2020).
 - ²³ L. Li, C. H. Lee, S. Mu, and J. Gong, Critical non-Hermitian Skin Effect, *Nature communications* **11**, 5491 (2020).
 - ²⁴ C. H. Lee, L. Li, and J. Gong, higher-order skin-topological modes in nonreciprocal systems, *Phys. Rev. Lett.* **123**, 016805 (2019).
 - ²⁵ W. D. Heiss, The physics of exceptional points, *J. Phys. A* **45**, 444016 (2012).
 - ²⁶ C. Dembowski, B. Dietz, H.-D. Gräf, H. L. Harney, A. Heine, W. D. Heiss, and A. Richter, "Encircling an exceptional point," *Phys. Rev. E* **69**, 056216 (2004).
 - ²⁷ I. Rotter, "A non-Hermitian Hamilton operator and the physics of open quantum systems," *J. Phys. A* **42**, 153001 (2009).
 - ²⁸ J.-W. Ryu, S.-Y. Lee, and S. W. Kim, "Analysis of multiple exceptional points related to three interacting eigenmodes in a non-Hermitian Hamiltonian," *Phys. Rev. A* **85**, 042101(2012).
 - ²⁹ W. Hu, H. Wang, P. P. Shum, and Y. D. Chong, "Exceptional points in a non-Hermitian topological pump," *Phys. Rev. B* **95**, 184306 (2017).
 - ³⁰ A. U. Hassan, B. Zhen, M. Soljacic, M. Khajavikhan, and D. N. Christodoulides, "Dynamically Encircling Exceptional Points: Exact Evolution and Polarization State Conversion," *Phys. Rev. Lett.* **118**, 093002 (2017).
 - ³¹ L. Pan, S. Chen, and X. Cui, High-order exceptional points in ultracold Bose gases, *Phys. Rev. A* **99**, 011601 (2019).
 - ³² Z. Gong, Y. Ashida, K. Kawabata, K. Takasan, S. Higashikawa, and M. Ueda, Topological Phases of Non-

- Hermitian Systems, *Phys. Rev. X* **8**, 031079 (2018).
- ³³ C.-H. Liu, H. Jiang, and S. Chen, Topological classification of non-Hermitian systems with reflection symmetry, *Phys. Rev. B* **99**, 125103 (2019).
- ³⁴ K. Kawabata, K. Shiozaki, M. Ueda, and M. Sato, Symmetry and topology in non-Hermitian physics, *Phys. Rev. X* **9**, 041015 (2019).
- ³⁵ H. Zhou and J. Y. Lee, Periodic table for topological bands with non-Hermitian symmetries, *Phys. Rev. B* **99**, 235112 (2019).
- ³⁶ C.-H. Liu, and S. Chen, Topological classification of defects in non-Hermitian systems, *Phys. Rev. B* **100**, 144106 (2019).
- ³⁷ Y. Ashida, Z. Gong, and M. Ueda, "Non-Hermitian Physics," arXiv:2006.01837(2020).
- ³⁸ F. Song, S. Yao, and Z. Wang, Non-Hermitian Skin Effect and Chiral Damping in Open Quantum Systems, *Phys. Rev. Lett.* **123**, 170401 (2019).
- ³⁹ C.-H. Liu, K. Zhang, Z. Yang, and S. Chen, Helical damping and dynamical critical non-Hermitian skin effect, *Phys. Rev. Research*, **2**, 043167 (2020).
- ⁴⁰ H. Hodaei, A.U. Hassan, S. Wittek, H. Garcia-Gracia, R. El-Ganainy, D.N. Christodoulides, and M. Khajavikhan, "Enhanced sensitivity at higher-order exceptional points," *Nature (London)* **548**, 187 (2017).
- ⁴¹ W. Chen, S.K. Özdemir, G. Zhao, J. Wiersig, and L. Yang, "Exceptional points enhance sensing in an optical microcavity," *Nature (London)* **548**, 192 (2017).
- ⁴² J. Wiersig, "Enhancing the Sensitivity of Frequency and Energy Splitting Detection by Using Exceptional Points: Application to Microcavity Sensors for Single-Particle Detection," *Phys. Rev. Lett.* **112**, 203901 (2014).
- ⁴³ J. Wiersig, "Sensors operating at exceptional points: General theory," *Phys. Rev. A* **93**, 033809 (2016)
- ⁴⁴ F. D. M. Haldane, "Model for a Quantum Hall Effect without Landau Levels: Condensed-Matter Realization of the "Parity Anomaly"," *Phys. Rev. Lett.* **61**, 2015 (1988).
- ⁴⁵ C. L. Kane and E. J. Mele, "Quantum spin hall effect in graphene," *Phys. Rev. Lett.* **95**, 226801 (2005).
- ⁴⁶ B. A. Bernevig, T. L. Hughes, and S.-C. Zhang, "Quantum Spin Hall Effect and Topological Phase Transition in HgTe Quantum Wells," *Science* **314**, 1757 (2006).
- ⁴⁷ L. Fu, C. L. Kane, and E. J. Mele, "Topological Insulators in Three Dimensions," *Phys. Rev. Lett.* **98**, 106803(2007).